RSC Advances

PAPER

View Article Online
View Journal | View Issue

Cite this: *RSC Adv.*, 2018, **8**, 37715

Fabrication of eco-friendly nanofibrous membranes functionalized with carboxymethyl-β-cyclodextrin for efficient removal of methylene blue with good recyclability†

Yinli Liu,[ab] Dequn Wu,*[ab] Xueli Wang,[c] Jianyong Yu[c] and Faxue Li*[abc]

Received 10th September 2018
Accepted 21st October 2018

DOI: 10.1039/c8ra07523a

rsc.li/rsc-advances

Considering the excellent thermo-mechanical properties, chemical stability and low cost of biodegradable aliphatic–aromatic copolyesters, they are an ideal matrix when functionalized for capturing pollutants in wastewater. In this work, biodegradable poly((butylene succinate-*co*-terephthalate)-*co*-serinol terephthalate) (PBSST) copolyesters with amino side group ($-NH_2$) were first synthesized through copolymerization, followed by grafting carboxymethyl-β-cyclodextrin (CM-β-CD) into PBSST molecular chains *via* amidation reaction to prepare PBSST-*g*-β-CD. The corresponding nanofibrous membranes were then fabricated by electrospinning as adsorbents for efficiently removing cationic dye methyl blue (MB) from aqueous solutions. The adsorption performance of the nanofibrous membranes was fitted well with pseudo-second-order model and Langmuir isotherm model. The maximum adsorption capacity was 543.48 mg g^{-1} for MB along with a removal efficiency of 98% after five regeneration cycles, indicating the high adsorption capacity and good recyclability of nanofibrous membranes. The adsorbents possess features of high adsorption capacity, eco-friendliness and easy operation, and exhibit great potential for disposing of printing-dying wastewater.

Introduction

Nowadays, various dyes are widely used in food, medicine, printing, dyeing, and cosmetics industries, so more and more organic and inorganic pollutants have been produced posing great threat to human health and the stability of the ecological environment. Various techniques including chemical precipitation,[1] photodegradation,[2] electro-chemical treatment,[3] evaporative recovery,[4] solvent extraction,[5] ultrafiltration,[6] ion exchange,[7] filtration,[8] adsorption,[9] and electrodialysis[10] have been utilized to remove pollutants from wastewater. Among these methods, adsorption is always confirmed to be an efficient route to capture organic and inorganic pollutants in the ecological water environment due to its easy operation, wide adaptability and excellent remediation. However, the application of some adsorbents is restricted due to their high cost,[11] low recyclability,[12] and low adsorption capacity.[13] Membrane technology is one of the most important and effective strategies for wastewater purification. Water separation through membrane technology is highly efficient, cost-effective, energy-saving, and eco-friendly. Nanofibrous membranes obtained *via* electrospinning as adsorbents for removing pollutants have become of interest because of their relatively simple fabrication and cost effectiveness,[14,15] and they can improve the adsorption capacity of substrate material.

Cyclodextrin (CD) is a cyclic oligosaccharide produced by starch under the action of amylase, and possesses a rigid, truncated-cone structure with a hydrophobic internal cavity and hydrophilic external surface, which can be utilized as a sustainable adsorbent for selectively encapsulating pollutants (various small molecules, polymers, ions, or even radicals, *etc.*) to form well-defined host-guest complexes.[16] Therefore, CD and its derivatives have been widely utilized to remove organic and inorganic pollutants, especially β-CD for application due to its wide availability, low cost and eco-friendliness. However, the solubility of β-CD in water limits its application in sewage purification,[17] so β-CD functionalized polymers have been studied intensively as adsorbents for removing pollutants.[18–22]

As a biodegradable aliphatic-aromatic copolyester, poly(-butylene succinate-*co*-terephthalate) (PBST) has excellent thermo-mechanical properties, chemical stability and

[a]*Key Laboratory of Textile Science & Technology, Ministry of Education, Donghua University, Shanghai 201620, China. E-mail: fxlee@dhu.edu.cn; dqwu@dhu.edu.cn*
[b]*College of Textiles, Donghua University, Shanghai 201620, China*
[c]*Innovation Center for Textile Science and Technology, Donghua University, Shanghai 201620, China*

† Electronic supplementary information (ESI) available: ^{1}H NMR spectra of serinol and N-BOC-serinol, PBST, PBSST5, PBSST7, PBSST10, PBSST20 and CM-β-CD. UV-vis spectra of MB solution adsorbed by PBSST20-*g*-β-CD nanofibrous membrane. Average diameters, contact angles and adsorption capacity of PBST, PBSST and PBSST-*g*-β-CD nanofibrous membranes. See DOI: 10.1039/c8ra07523a

resistance to deformation,[23–25] and is an ideal matrix functionalized for capturing pollutants in wastewater. Recently, we fabricated PBST nanofibrous membranes physically compounded with β-CD, which is used to adsorb the cationic dye methyl blue (MB) in aqueous solution and the maximum adsorption capacity is 90.9 mg g^{-1}.[26] After the service life is terminated, the membranes can be biodegraded in soil without secondary pollution. Nevertheless, the prepared membranes have poor adsorption capacity and low recyclability since the β-CD derivatives cannot be chemically linked with PBST nanofibrous membranes at the absence of reactive functional groups in PBST molecular chains, which results into easily peeling-off of β-CD derivatives from the matrix. In addition, the porous structure of PBST nanofibrous membranes is destroyed by β-CD physically coated on the surface of nanofibrous membranes, resulting in the poor adsorption capacity of PBST nanofibrous membranes physically compounded with β-CD. Therefore, it is necessary to immobilize β-CD or its derivatives on the surface of PBST nanofibrous membranes to improve the adsorption capacity and extend the recyclability of adsorbents in wastewater purification.

In this work, novel PBSST copolyesters with amino side group ($-NH_2$) were first synthesized on the basis of PBST synthesis, followed by grafting carboxymethyl-β-cyclodextrin (CM-β-CD) into the copolyesters *via* amidation reaction between amino groups of PBSST and carboxyl groups of CM-β-CD to prepare the eco-friendly materials (the schematic diagram of synthesis route of PBSST-*g*-β-CD in Fig. 1). The corresponding nanofibrous membranes were then fabricated *via* electrospinning to adsorb MB in aqueous solutions, and they showed large adsorption capacity to MB with good recyclability. The experiment results indicate that the PBSST-*g*-β-CD nanofibrous membranes present a great potential in disposing the printing-dying wastewater.

Experimental section

Materials

Dimethyl terephthalate (DMT), dimethyl succinate (DMS), 1,4-butanediol (BD), chloroform and dichloromethane (DCM), sodium hydroxide (NaOH) and hydrochloric acid (HCl) were commercially supplied by Shanghai Lingfeng Chemical Reagent Co. Ltd. Serinol was supplied by Shanghai Yijing industrial Co. Ltd. Sodium chloride (NaCl) was supplied by Sinopharm Chemical Reagent Co. Ltd. Tetrabutyl titanate (TBT), ditertbutyl dicarbonate ($(Boc)_2O$), sulfamic acid, methylene blue (MB), 1-ethyl-3-(3-dimethyl aminopropyl) carbodiimide hydrochloride (EDC), hexafluoroisopropanol (HFIP) and *N*-hydroxysuccinimide (NHS) were supplied by Aladdin Chemical Regents Co. Ltd. Carboxymethyl-β-cyclodextrin (CM-β-CD) was supplied by Zhiyuan Bio-Technology Co. Ltd (Shandong, China). All chemicals were of analytical grade and used as received without further purification.

Preparation of N-BOC-serinol

N-BOC protection of serinol was catalyzed by sulfamic acid under the followed conditions. $(Boc)_2O$ (1.1 mol) and sulfamic acid (0.05 mol) were put in 500 mL round-bottom flask at 25 °C. Serinol (1 mol) was added into the flask with stirring at 55 °C for 15 min. Saturated NaCl aqueous solution (100 mL) and ethyl acetate (150 mL) were put in the reaction mixture, and then aqueous and organic layers appeared. The aqueous layer was extracted with ethyl acetate (150 mL) for three times, while the organic layer were collected, dried with $MgSO_4$, and then concentrated.

Preparation of N-BOC-PBSST copolyesters

In order to increase the conversion rate of monomer, N-BOC-PBSST copolyesters were synthesized with the stepwise method with DMT, DMS, BD and N-BOC-serinol. DMT (0.2 mol), DMS (0.2 mol), BD (0.42 mol) and TBT with a certain fraction were mixed together in a round-bottom flask and stirred at about 200 °C for 2–3 h to gain Ester 1. DMT (0.2 mol), N-BOC-serinol (0.21 mol) and TBT with a certain fraction were mixed together in a round-bottom flask and stirred at about 180 °C for 2–3 h to gain Ester 2. Subsequently, Ester 1 and Ester 2 were mixed together with different molar ratios (5%, 7%, 10%, 20% of Ester 2 to Ester 1), and heated to 210 °C at a pressure of 70 kPa with stirring for 2 h. Then the polycondensation occurred under the gradually reduced pressure and increasing temperature to 230 °C. The reaction was terminated as the stirrer torque approached the maximum. The as-products were dissolved in chloroform, and then precipitated from cold methanol for purification. Then white solid products were collected after drying under high vacuum overnight.

Deprotection of N-BOC-PBSST copolyesters

N-BOC-PBSST copolyesters (10 g) were dissolved in anhydrous chloroform (200 mL) at room temperature and bubbled with HCl for 2 h. The resulting solution was added dropwise into cold methanol and then precipitated. White solid products (PBSST) were obtained after dried to constant weight for the next grafting reaction.

Synthesis of PBSST-*g*-β-CD copolymers

CM-β-CD (8.000 g), EDC (0.863 g) and NHS (1.436 g) were dissolved in 100 mL of HFIP aqueous solution (90 v/v%). The reaction was stirred in ice bath for 6 h before PBSST was added with stirring for another 6 h at room temperature. The resulting solution was added dropwise into cold methanol and reprecipitated to obtain white solid products. The products were thoroughly washed with hot deionized water for several times. Then white solid products were received after dried to constant weight.

Fabrication of nanofibrous membranes

PBST, PBSST and PBSST-*g*-β-CD nanofibrous membranes were fabricated through electrospinning. The as-products were dissolved in DCM to prepare 20 wt% spinning solutions with stirring for 12 h continuously. The spinning solution was loaded into syringe with a metallic needle (inner diameter 0.5 mm), and high voltage of 16 kV, feed rate of 1.5 mL h^{-1}, the distance

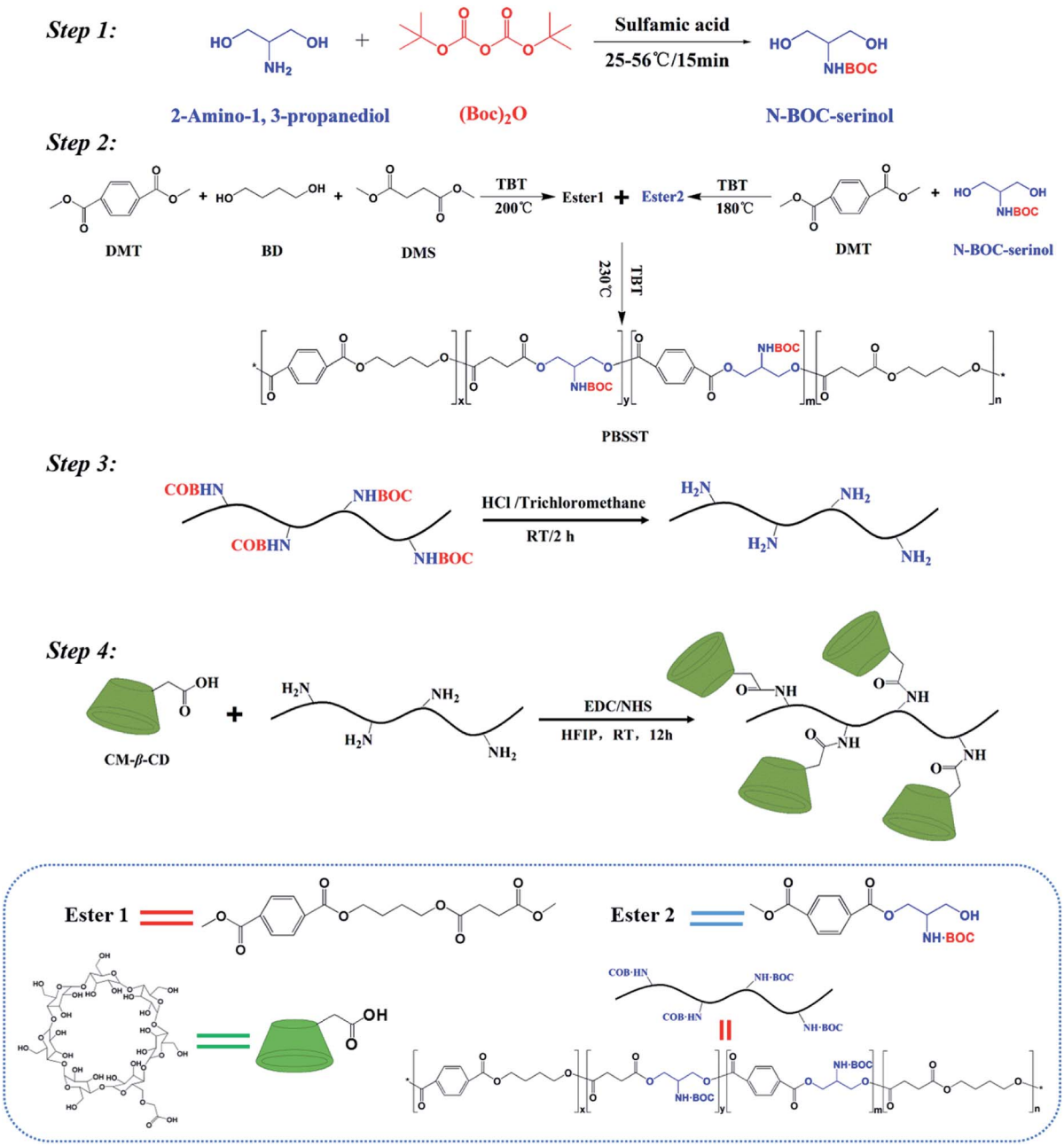

Fig. 1 Schematic diagram of the synthesis of PBSST-*g*-β-CD.

between needle tip and collector of 15 cm were applied to perform electrospinning. The temperature and relevant humidity were kept at 25 °C and 35%, respectively.

Characterization

Microstructures of as-prepared products were characterized by different techniques. Nuclear magnetic resonance (^{1}H NMR, AVANCE400, Bruker) spectra were recorded with the resonance frequency of 400 MHz. Fourier transform infrared spectroscopy (FTIR) analyzer (Nicolet 6700, Thermo Fisher) equipped with the Smart iTR operated on the attenuated total reflectance (ATR) mode in the wave-number range of 4000–400 cm^{-1}. X-ray diffraction (XRD, max-2550VB, Rigaku) patterns were collected using a diffractometer with a Cu-Kα source (λ = 1.5418 Å). Differential scanning calorimetry (DSC4000, PerkinElmer) and thermogravimetric analysis (TGA4000, PerkinElmer) were used to investigate the thermal properties of PBST and PBSST. The morphologies of nanofibrous membranes were examined by scanning electron microscopy (SEM, JSM-5600LV, JEOL) at an accelerating voltage of 10 kV. The water contact angles of the nanofibrous membranes were measured by using a contact angle goniometer (OCA15EC, Dataphysics Instruments).

Adsorption–desorption studies

Adsorption experiments were performed on a model BETS-M1 shaker (Kylin-Bell Lab Instruments Co. Ltd, China) with

a shaking speed of 120 rpm at room temperature. The pH values of MB solution were adjusted by a pH meter with adding small amount of 0.1 mol L^{-1} HCl or 0.1 mol L^{-1} NaOH solution. PBST, PBSST and PBSST-*g*-β-CD nanofibrous membranes were individually immersed in MB solution with initial concentration of 10 mg L^{-1} and desired pH value of 2–12 for a certain time at room temperature; 50 mg of PBSST-*g*-β-CD nanofibrous membranes were immersed in MB solution (10 mg L^{-1}, pH = 9) at different times (0–120 min) to explore the adsorption kinetics; 50 mg of PBSST-*g*-β-CD nanofibrous membranes were immersed in MB solution with different initial concentrations (5–200 mg L^{-1}, pH = 9) to reveal the adsorption isotherms.

For desorption experiment, PBSST-*g*-β-CD nanofibrous membranes adsorbed MB were washed with deionized water, then were put into methanol solution containing 5% (v/v) HCl (0.1 mol L^{-1}) solution. After desorption equilibrium, the membranes were washed for several times with deionized water and reused for MB adsorption (adsorbent, 50 mg; MB solution, 50 mL, 50 mg L^{-1}, initial pH = 9). The adsorption–desorption process was repeated for 5 times. The concentration of MB solution was measured by a UV-vis spectroscopy (UV-2550, Shimadzu) at the wavelength of 665 nm. MB removal efficiency (R_t) and adsorption capacity (q_t) at time t were determined *via* the following equations respectively:

$$R_t = 100 \times (C_0 - C_t)/C_0$$

$$q_t = V \times (C_0 - C_t)/W$$

where R_t(%) is dye removal efficiency at time t and q_t is the adsorption capacity at time t (mg g^{-1}); C_0 is the initial concentration and C_t is the concentration of MB solution at time t (mg L^{-1}); V is the volume of MB solution (L); W is the mass of absorbent (g). All the experimental data are the average of duplicate determinations, and 5% relative errors are provided in some measurements. The schematic diagram of MB adsorption on nanofibrous membranes is shown in Fig. 2.

Results and discussion

Characterization of raw materials and synthetic products

Fig. 3 plots the ^{1}H NMR spectra of PBSST20 and PBSST20-*g*-β-CD, where "20" means the feed ratio of Ester 2 to Ester 1 is

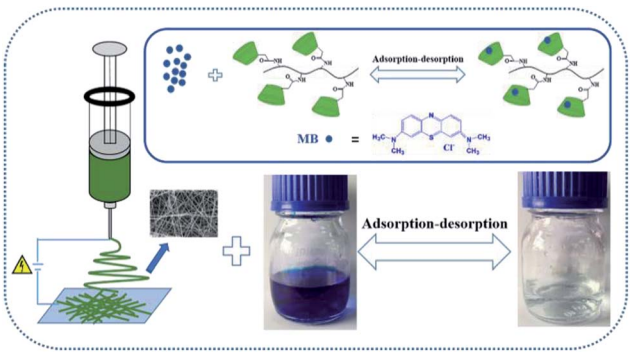

Fig. 2 Schematic diagram of MB adsorption on the nanofibrous membranes.

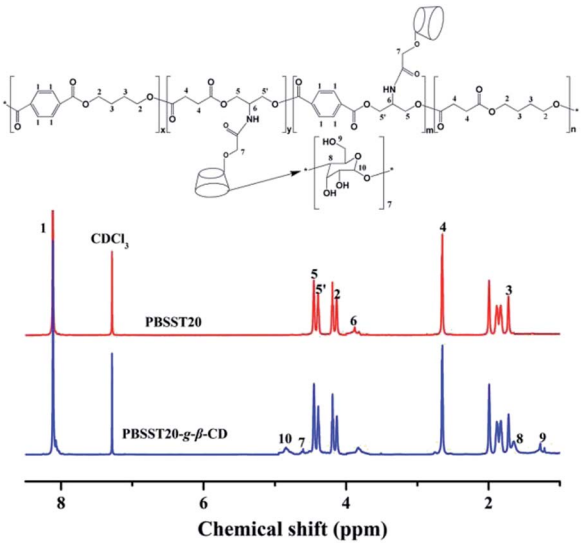

Fig. 3 ^{1}H NMR spectra of PBSST20 and PBSST20-*g*-β-CD.

20 mol% (the same meaning in other PBSST copolyesters). Peak at 3.8 ppm ((6) –CH–NH–) for PBSST20 corresponding to the hydrogen proton of methyne (–CH) of serinol appears (Fig. S1(a and b)†), indicating serinol unit is introduced into the molecular chains successfully. According to ^{1}H NMR results in Fig. S1,† conversion ratio of N-BOC-serinol is calculated to be 75%, 73%, 73% and 72% for PBSST5, PBSST7, PBSST10 and PBSST20 respectively as listed in Table 1. Furthermore, new peaks appear at 4.82 ppm ((10) –O–CH–O–), 4.59 ppm ((7) –O–CH_2–CO–), 1.68 ppm ((8) –CH–CH–) and 1.25 ppm ((9) –CH) for PBSST20-*g*-β-CD in $CDCl_3$, indicative of the formation of covalent bonds between CM-β-CD and PBSST20.

FTIR spectra of serinol, N-BOC-serinol, PBST, PBSST, CM-β-CD and PBSST-*g*-β-CD are shown in Fig. 4(a–c), and the absorption bands of serinol at about 3410 cm^{-1} correspond to the stretching vibrations of –OH, N–H, and those at about 2960 cm^{-1} correspond to the stretching vibration of –CH. Compared to serinol, new absorption bands appear at about 1686, 1531 and 1250 cm^{-1} in the spectrum of N-BOC-serinol, which are attributed to the stretching vibrational modes of C=O, N–H and C–O–C respectively.[27] Different from PBST spectrum, the stretching vibration of N–H at around 3360 and 1656 cm^{-1} can be observed in the spectra of PBSST copolyesters, confirming the N-BOC-serinol involved in the copolymerization. This is in accordance with the results obtained from ^{1}H NMR. New absorption bands at around 1643, 1539 cm^{-1} for PBSST-*g*-β-CD are the indication of C=O and N–H groups formation, confirming that CM-β-CD is chemically grafted into PBSST through amide bonds. In addition, the as-prepared PBSST-*g*-β-CD shows the absorption bands of oxygen-containing functional groups stretching vibrations of CM-β-CD such as –OH (3410 cm^{-1}),[28] which further verifies that the grafting reaction between CM-β-CD and PBSST occurs.

Fig. 4(d) displays the XRD curves of PBST and PBSST. It is obvious that the XRD patterns of PBSST have similar diffraction peaks at 17.2° (010), 20.2° (101), 23.2° (100) to PBST, indicating that the crystal structures of PBSST do not alter significantly

Table 1 Thermal properties and crystallinities of PBST and PBSST

Sample	Conversion ratio of N-BOC-serinol (%)[a]	T_m (°C)	T_d (°C)	Crystallinity (%)[b]
PBST	—	140	370	14.23
PBSST5	75	136	364	11.43
PBSST7	73	133	362	11.16
PBSST10	73	130	359	10.84
PBSST20	72	126	356	4.70

[a] Conversion ratio is determined by calculating the area ratio of peak at 3.8 ppm to peak at 2.64 ppm in Fig. S1. [b] Crystallinity is determined by fitting the XRD curves through Origin software.

with the introduction of N-BOC-serinol unit. However, the intensities of diffraction peaks of PBSST are reduced with the increasing feed ratio of N-BOC-serinol, indicating the crystallinity decreases due to the increasing atacticity as shown in Table 1.

DSC and TGA measurements were conducted to investigate the thermal properties of PBST and PBSST as shown in Fig. 4(e and f). It can be seen that melting temperature (T_m) decreases from 140 °C to 126 °C and decomposition temperature (T_d) decreases from 370 °C to 356 °C with the increasing feed ratio of N-BOC-serinol since the structure tacticity of copolymers is deteriorated with the introduction of new comonomer.

SEM technique was applied to investigate the morphological structures of PBST, PBSST and PBSST-*g*-β-CD nanofibrous membranes as shown in Fig. 5. The nanofibrous membranes are randomly oriented and the average diameter of fibers decreases to 469 nm from 653 nm (listed in Table S1†) with the increasing feed ratio of N-BOC-serinol. Actually, the effect of conductance of solution on the diameter of single nanofiber is a critical factor. In the research, the content of amino groups ($-NH_2$) increases with the increasing feed ratio of N-BOC-serinol, which causes the increase of conductance of solution. In addition, the electrostatic repulsion among nanofibers increase with the increasing content of amino groups ($-NH_2$), which causes the decrease of diameter of fibers.[29,30]

The contact angles of nanofibrous membranes influence their adsorption capacity to MB. As seen in Table S1,† the hydrophobic PBST nanofibrous membrane has the water contact angle of 135°, while the contact angles of PBSST nanofibrous membranes are reduced to 102° from 129° with the increasing feed ratio of N-BOC-serinol. After grafted with CM-β-CD, the prepared nanofibrous membranes have the sharply decreasing contact angle from 98° of PBSST5-*g*-β-CD nanofibrous membrane to 46° of PBSST20-*g*-β-CD nanofibrous membrane, indicating that the as-prepared PBSST20-*g*-β-CD membrane is hydrophilic, which in turn is beneficial to the MB adsorption in aqueous solution.

Overall, combining the results from characterization, one can concluded that CM-β-CD is chemically grafted into PBSST with covalent bonding, while the fabricated PBSST20-*g*-β-CD nanofibrous membrane has good hydrophilic and abundant active sites for the removal of pollutants in wastewater. Hence,

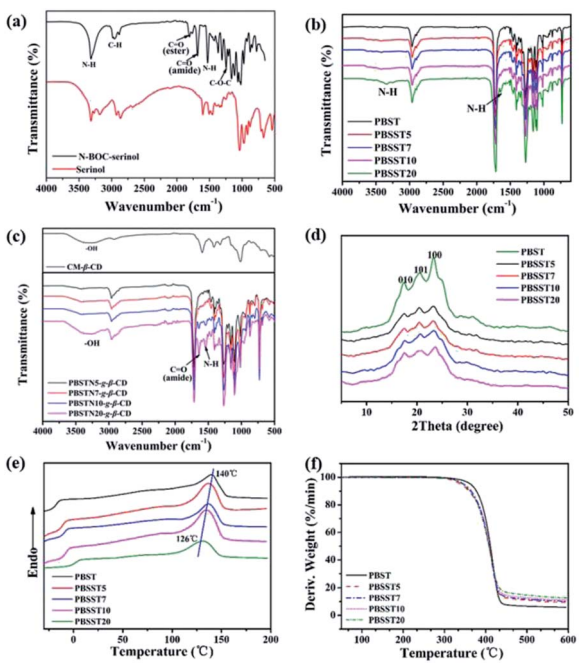

Fig. 4 (a–c) FTIR spectra of serinol and N-BOC-serinol, PBST and PBSST, CM-β-CD and PBSST-*g*-β-CD; (d) XRD curves of PBST and PBSST; (e) DSC curves of PBST and PBSST; (f) TGA curves of PBST and PBSST.

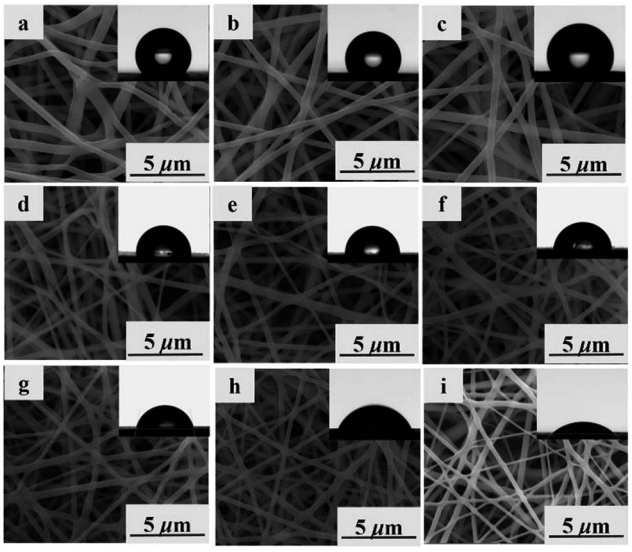

Fig. 5 Representative SEM images of nanofibrous membranes fabricated with solutions of (a) PBST; (b) PBSST5; (c) PBSST7; (d) PBSST10; (e) PBSST20; (f) PBSST5-*g*-β-CD; (g) PBSST7-*g*-β-CD; (h) PBSST10-*g*-β-CD; (i) PBSST20-*g*-β-CD. Contact angle image of each sample is attached on the top right corner of SEM image.

PBSST20-*g*-β-CD nanofibrous membrane is selected for the MB adsorption in the following research.

Adsorption experiments

Effects of adsorbent amount. As a novel adsorbent, the added amount of PBSST20-*g*-β-CD nanofibrous membrane has been considered in the adsorption of MB, and the corresponding result is displayed in Fig. 6(a). The R_t value of adsorbent to MB increases from 15% to 99% with increasing the used adsorbent amount from 0.02 g L^{-1} to 0.1 g L^{-1} in MB solution since more surface adsorption sites are available to capture MB molecules through the abundant oxygen-containing functional groups of β-CD, which adsorbs MB completely and the R_t value of adsorbent to MB will be hardly changed with the increase of the adsorbent amount.

Effect of pH value of MB solution. Fig. 6(b) plots the R_t change of PBSST20-*g*-β-CD nanofibrous membrane to MB in different solution pH values with initial concentration of 10 mg L^{-1}. The R_t value increases with the increasing solution pH value from 2 to 9 and decreases at pH value of 9 to 12. As the pH value of MB solution is 9, the R_t value approaches the maximum. This phenomenon can be explained by the change of interaction between MB molecules and nanofibrous membrane. At low pH values, the adsorption sites of nanofibrous membrane and dimethylamine group of MB are protonated, which results in electrostatic repulsion between MB molecules and nanofibrous membrane. The existence of electrostatic interaction restricts the interaction between MB molecules and nanofibrous membrane, therefore the adsorption capacity of nanofibrous membrane to MB declines at low pH value. With the pH value increasing, the electrostatic repulsion is weakened with the decrease of protonation, thus more MB molecules are adsorbed onto the nanofibrous membrane by van der Waals and hydrogen bonds.[31]

However, as the pH value of MB solution is higher than 9, the electrostatic repulsion between deprotonated adsorption sites of nanofibrous membrane and deprotonated dimethylamine group of MB restricts the interaction between MB molecules and nanofibrous membrane.[31] Therefore, the R_t decreases with the continued increasing pH value of MB solution. These results suggest that the pH value of MB solution is significant to determine the removal efficiency of nanofibrous membrane to MB. Therefore, the adsorption process is dominated not only by the host-guest inclusion with the specific cavum from cyclodextrin derivative, but also the electrostatic interaction between hydroxy groups from nanofibrous membrane and groups containing nitrogen of MB molecules, which can be attributed to hydrogen bonds and van der Waals forces.

Sorption kinetics. Sorption kinetics of PBSST20-*g*-β-CD nanofibrous membrane to MB was investigated at different adsorption times as shown in Table S2† and Fig. 7(a and b). It can be found that the adsorption capacity increases rapidly with prolonging the adsorption time and reaches the plateau within 20 min. The maximum R_t reaches 99% after adsorption for 40 min, demonstrating high adsorption efficiency of PBSST20-*g*-β-CD membrane to MB molecules. The UV-vis spectra of MB solution adsorbed by PBSST20-*g*-β-CD nanofibrous membrane at different time intervals are shown in Fig. S2.†

To further study the adsorption process (*e.g.*, mass transfer or chemical reaction), the kinetic data were fitted by pseudo-first-order and pseudo-second-order kinetic models. The pseudo-first-order kinetic model eqn (1) and pseudo-second-order kinetic model eqn (2) are usually given as followed:[32]

Pseudo-first order:

$$q_t = q_e(1 - e^{-k_1 t}) \quad (1)$$

Pseudo-second order:

$$\frac{t}{q_e} = \frac{1}{k_2 q_e^2} + \frac{t}{q_e} \quad (2)$$

where k_1 is the pseudo-first order rate constant (min^{-1}) and k_2 presents the pseudo-second order rate constant (g mg^{-1} min^{-1}); q_t and q_e are the adsorption capacity at time t and equilibrium state (mg g^{-1}), respectively. As shown in Fig. 7(b), the high linearity ($R^2 > 0.99$) of fitting curve indicates that the adsorption of PBSST-*g*-β-CD nanofibrous membrane to MB follows the pseudo-second-order model. The pseudo-second-order model is based on the assumption that the rate-limiting step may be a chemical process that involves valance forces through sharing or exchanging electrons between adsorbents and adsorbates, and it indicates that the adsorption behaviour is dominated by a chemical adsorption process in this work.[33]

Adsorption isotherm and cycle adsorption. Two well-known isotherm models (Langmuir and Freundlich) were applied to simulate the adsorption isotherms for the purpose of evaluating the adsorption behaviour of PBSST-*g*-β-CD nanofibrous membrane for MB, which are expressed as:

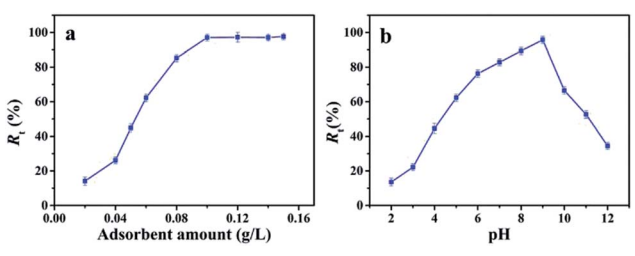

Fig. 6 R_t variation *versus* adsorbent amount in MB solution (a), and pH value of MB solution (b).

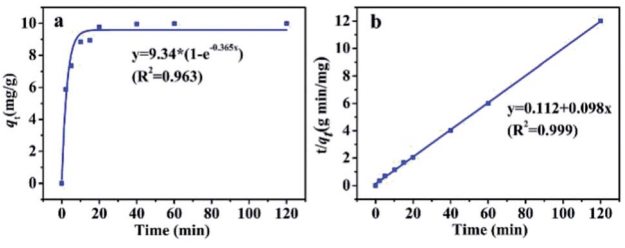

Fig. 7 Adsorption kinetics plots of PBSST20-*g*-β-CD nanofibrous membrane to MB: (a) pseudo-first order fitting; (b) pseudo-second order fitting.

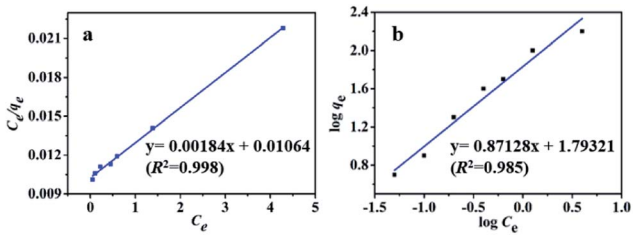

Fig. 8 Adsorption isotherm and the corresponding Langmuir plot (a) and Freundlich plot (b) for MB adsorbed by PBSST20-*g*-β-CD nanofibrous membrane.

Langmuir model:

$$\frac{C_e}{q_e} = \frac{1}{bq_m} + \frac{C_e}{q_m} \quad (3)$$

Freundlich model:

$$\log q_e = \log k_F + \frac{1}{n} \log C_e \quad (4)$$

where C_e is the concentration at adsorption equilibrium (mg L^{-1}); q_e is the equilibrium adsorption capacity of MB adsorbed by PBSST20-*g*-β-CD nanofibrous membrane (mg g^{-1}); b is equilibrium constant that is associated with the energy of adsorption (L mg^{-1}); q_m is the maximum adsorption capacity of MB (mg g^{-1}); K_F and n are empirical constants indicating the Freundlich constant (L mg^{-1}) and heterogeneity factor, respectively.

MB adsorption isotherm is displayed in Fig. 8(a and b) and the corresponding parameters calculated from the two models are listed in Table 2. Obviously, MB adsorption isotherm is well fitted by the Langmuir model ($R^2 > 0.99$), showing that the MB adsorption on PBSST20-*g*-β-CD nanofibrous membrane is mainly a monolayer adsorption and relatively homogeneous. The maximum adsorption capacity (q_m) of MB onto PBSST20-*g*-β-CD nanofibrous membrane calculated from the Langmuir model is 543.48 mg g^{-1}, significantly higher than PBST and PBSST nanofibrous membranes shown in Table 2, indicating the introduction of the cavum from cyclodextrin is very beneficial to the MB adsorption. It is also interesting to found that the maximum adsorption capacity of PBSST nanofibrous membranes to MB is increased with the increasing feed ratio of serinol, suggesting that the increase of amino group ($-NH_2$) in PBSST is propitious to MB adsorption due to the formation of hydrogen bonds between MB and PBSST nanofibrous membrane. Meanwhile, PBSST20-*g*-β-CD nanofibrous membrane has significantly higher q_m value than the available adsorbents reported in literatures as listed in Table 3. The high adsorption capacity of PBSST20-*g*-β-CD nanofibrous membrane is contributed to the peculiar hydrophobic cavum of cyclodextrin, which can capture MB molecules by host-guest complexes. In addition, the porous structure in the nanofibrous membrane can adsorb the MB molecules to some extent. The synergy of the two factors is contributed to the high adsorption capacity.

Table 3 Comparison of the maximum adsorption capacity (q_m) of MB with other adsorbents

Adsorbent	q_m (mg g^{-1})	Reference
β-CD/PAA/GO	247.99	34
PVA-SS-CD	187.27	35
PBST/CDP	90.90	26
HNT-CD (40%) hybrid	226.00	36
PBSST-*g*-β-CD	543.48	This work

Reusability of adsorbent is essential for protecting ecological environment and reducing the overall cost in practical applications. Thus multiple experiments were conducted to demonstrate the good recyclability of PBSST20-*g*-β-CD nanofibrous membrane. As shown in the above study, PBSST20-*g*-β-CD nanofibrous membrane tends to adsorb few MB molecules at a low pH value, so methanol solution containing 5% (v/v) HCl (0.1 mol L^{-1}) was used to regenerate the MB-adsorbed PBSST20-*g*-β-CD nanofibrous membrane. In this research, the adsorption–desorption cycle was repeated five times and the results are presented in Fig. 9. It can be seen that the R_t value remains at 98% after five regeneration cycles, which suggests that PBSST20-*g*-β-CD nanofibrous membrane has good recyclability in MB adsorption–desorption. Hence the prepared β-cyclodextrin-included nanofibrous membrane is a good candidate for efficiently removing MB in the printing-dying wastewater.

Adsorption mechanism and simulation. Fig. 10 displays the optimized geometries for CM-β-CD, MB, PBSST, PBSST-*g*-β-CD and MB-adsorbed PBSST-*g*-β-CD *via* Material Studio software to further explain the adsorption mechanism of PBSST-*g*-β-CD nanofibrous membrane to MB. The geometrical dimensions of cyclodextrin cavity (top 7.690 Å bottom 17.061 Å) and MB molecule (width 5.017 Å, length 12.179 Å) are determined

Table 2 Langmuir and Freundlich isotherm fitting parameters for MB adsorption by PBST, PBSST, and PBSST20-*g*-β-CD nanofibrous membranes

	Langmuir isotherm			Freundlich isotherm		
Adsorbent (nanofibrous membranes)	q_m (mg g^{-1})	b (L mg^{-1})	R^2	K_F	n	R^2
PBST	49.90	0.048	0.996	3.18	1.73	0.933
PBSST5	55.80	0.045	0.996	3.24	1.67	0.937
PBSST7	62.20	0.040	0.997	3.26	1.63	0.945
PBSST10	67.60	0.038	0.998	3.40	1.61	0.955
PBSST20	74.20	0.036	0.998	3.44	1.56	0.957
PBSST20-*g*-β-CD	543.48	0.173	0.998	62.12	1.15	0.985

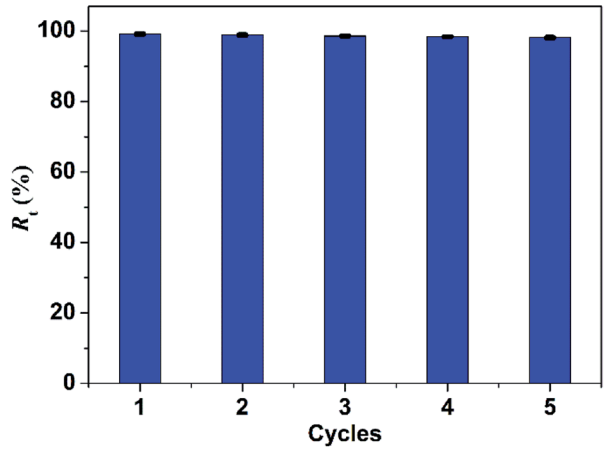

Fig. 9 Adsorption–desorption cycles of PBSST20-*g*-β-CD nanofibrous membrane to MB.

through the software. The molecule dimension demonstrates that MB molecules can be included in the cavity of CM-β-CD grafted in PBSST-*g*-β-CD nanofibrous membrane, forming well-defined host-guest complexes. As shown in the figure, a series of hydrogen bonds[37,38] with the dimension of 2.560 Å, 2.819 Å, 3.105 Å, 2.970 Å, 3.125 Å were formed with the H, N atoms in MB and O, H atoms in the cavity of CM-β-CD. Combining the results from adsorption experiments, one can conclude that PBSST-*g*-β-CD nanofibrous membrane has high adsorption capacity to MB and the adsorption mechanism of MB on the nanofibrous membrane is dominated by the hydrogen bonds, electrostatic interactions and surface complexation.

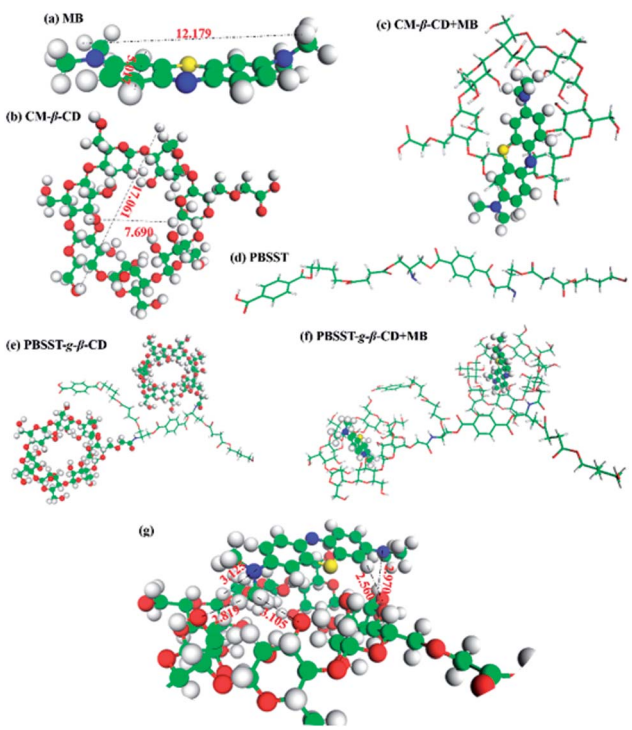

Fig. 10 Optimized geometries for CM-β-CD (a), MB (b), CM-β-CD + MB (c), optimized structures for PBSST (d), PBSST-*g*-β-CD (e), PBSST-*g*-β-CD + MB (f) and section of PBSST-*g*-β-CD + MB (g).

Conclusions

Novel eco-friendly PBSST-*g*-β-CD nanofibrous membranes were fabricated as adsorbents for removing MB from aqueous solutions. The results of adsorption experiment indicated that adsorption process of MB was well fitted with the pseudo-second order kinetic model and the Langmuir isotherm model. The maximum adsorption capacity was 543.48 mg g^{-1} for MB, much higher than many other adsorbents. After five regeneration cycles, MB removal efficiency still remained at 98%, suggesting that the nanofibrous membranes had good recyclability. The excellent adsorption of PBSST-*g*-β-CD nanofibrous membranes shows that they are promising materials for possible application in disposing printing-dying wastewater.

Conflicts of interest

There are no conflicts to declare.

Acknowledgements

This research was financially supported by Natural Science Fund of Shanghai City (18ZR1400500) and Application Fundamental Projects of China National Textile and Apparel Council.

Notes and references

1 N. Meunier, P. Drogui, C. Montane, R. Hausler, G. Mercier and J. F. Blais, *J. Hazard. Mater.*, 2006, **137**, 581–590.
2 Y. Feng, N. Feng, Y. Wei and G. Zhang, *RSC Adv.*, 2014, **4**, 7933.
3 R.-F. Yu, C.-H. Lin, H.-W. Chen, W.-P. Cheng and M.-C. Kao, *Chem. Eng. J.*, 2013, **218**, 341–349.
4 L. Chen, D. Huang, S. Ren, T. Dong, Y. Chi and G. Chen, *Nanoscale*, 2013, **5**, 225–230.
5 A. L. Ahmad, S. Sumathi and B. H. Hameed, *Chem. Eng. J.*, 2006, **118**, 99–105.
6 F. Peng, T. Luo and Y. Yuan, *New J. Chem.*, 2014, **38**, 4427.
7 C. Zhang, J. Hu, X. Wang, H. Toyoda, M. Nagatsu, X. Zhang and Y. Meng, *J. Power Sources*, 2012, **198**, 112–116.
8 H. Wang, L. Ma, K. Cao, J. Geng, J. Liu, Q. Song, X. Yang and S. Li, *J. Hazard. Mater.*, 2012, **229–230**, 321–330.
9 Y. Zou, X. Wang, Y. Ai, Y. Liu, J. Li, Y. Ji and X. Wang, *Environ. Sci. Technol.*, 2016, **50**, 3658–3667.
10 R. Hu, X. Wang, S. Dai, D. Shao, T. Hayat and A. Alsaedi, *Chem. Eng. J.*, 2015, **260**, 469–477.
11 D. Li, Q. Li, D. Mao, N. Bai and H. Dong, *Bioresour. Technol.*, 2017, **245**, 649–655.
12 X. Gong, D. Huang, Y. Liu, G. Zeng, R. Wang, J. Wei, C. Huang, P. Xu, J. Wan and C. Zhang, *Bioresour. Technol.*, 2018, **253**, 64–71.
13 Y. Jiang, B. Liu, J. Xu, K. Pan, H. Hou, J. Hu and J. Yang, *Carbohydr. Polym.*, 2018, **182**, 106–114.
14 J. Xiao, W. Lv, Y. Song and Q. Zheng, *Chem. Eng. J.*, 2018, **338**, 202–210.
15 M.-Y. Lim, Y.-S. Choi, J. Kim, K. Kim, H. Shin, J.-J. Kim, D. M. Shin and J.-C. Lee, *J. Membr. Sci.*, 2017, **521**, 1–9.

16 L. Szente and J. Szeman, *Anal. Chem.*, 2013, **85**, 8024–8030.
17 E. M. M. Del Valle, *Process Biochem.*, 2004, **39**, 1033–1046.
18 A. I. Schäfer, K. Stelzl, M. Faghih, S. Sen Gupta, K. R. Krishnadas, S. Heißler and T. Pradeep, *ACS Sustainable Chem. Eng.*, 2017, **6**, 2942–2953.
19 N. Morin-Crini and G. Crini, *Prog. Polym. Sci.*, 2013, **38**, 344–368.
20 D. M. Alzate-Sánchez, B. J. Smith, A. Alsbaiee, J. P. Hinestroza and W. R. Dichtel, *Chem. Mater.*, 2016, **28**, 8340–8346.
21 M. Forouharshad, M. Putti, A. Basso, M. Prato and O. Monticelli, *ACS Sustainable Chem. Eng.*, 2015, **3**, 2917–2924.
22 A. Leudjo Taka, K. Pillay and X. Yangkou Mbianda, *Carbohydr. Polym.*, 2017, **159**, 94–107.
23 F. Li, S. Luo, J. Zhang and J. Yu, *J. Therm. Anal. Calorim.*, 2012, **113**, 915–921.
24 S. Luo, F. Li, J. Yu and A. Cao, *J. Appl. Polym. Sci.*, 2012, **125**, 2426–2432.
25 J. Zhang, X. Wang, F. Li and J. Yu, *Fibers Polym.*, 2012, **13**, 1233–1238.
26 Z. Wei, Y. Liu, H. Hu, J. Yu and F. Li, *RSC Adv.*, 2016, **6**, 108240–108246.
27 E. Busto, V. Gotor-Fernández, J. Montejo-Bernardo, S. García-Granda and V. Gotor, *Tetrahedron*, 2009, **65**, 8393–8401.
28 A. Z. M. Badruddoza, G. S. S. Hazel, K. Hidajat and M. S. Uddin, *Colloids Surf., A*, 2010, **367**, 85–95.
29 J. Ju, Z. Shi, L. Fan, Y. Liang, W. Kang and B. Cheng, *Mater. Lett.*, 2017, **205**, 190–193.
30 S. Haider, F. F. Binagag, A. Haider and W. A. Al-Masry, *J. Polym. Res.*, 2014, **21**, 371.
31 R. Zhao, Y. Wang, X. Li, B. Sun and C. Wang, *ACS Appl. Mater. Interfaces*, 2015, **7**, 26649–26657.
32 Q. Liu, L. B. Zhong, Q. B. Zhao, C. Frear and Y. M. Zheng, *ACS Appl. Mater. Interfaces*, 2015, **7**, 14573–14583.
33 Y. Zou, X. Wang, Y. Ai, Y. Liu, Y. Ji, H. Wang, T. Hayat, A. Alsaedi, W. Hu and X. Wang, *J. Mater. Chem. A*, 2016, **4**, 14170–14179.
34 J. Liu, G. Liu and W. Liu, *Chem. Eng. J.*, 2014, **257**, 299–308.
35 R. Zhao, Y. Wang, X. Li, B. Sun, Z. Jiang and C. Wang, *Colloids Surf., B*, 2015, **136**, 375–382.
36 M. Massaro, C. G. Colletti, G. Lazzara, S. Guernelli, R. Noto and S. Riela, *ACS Sustainable Chem. Eng.*, 2017, **5**, 3346–3352.
37 J. N. Eildal, G. Hultqvist, T. Balle, N. Stuhr-Hansen, S. Padrah, S. Gianni, K. Stromgaard and P. Jemth, *J. Am. Chem. Soc.*, 2013, **135**, 12998–13007.
38 C. H. Wu, K. Ito, A. M. Buytendyk, K. H. Bowen and J. I. Wu, *Biochemistry*, 2017, **56**(33), 4318–4322.